

# A novel approach to the localization and the estimate of radioactivity in contaminated waste packages via imaging techniques

Michele Pastena<sup>a,b,\*</sup>, Bastian Weinhorst<sup>a,b</sup>, Günter Kanisch<sup>c</sup>, Edgar Pérez Lezama<sup>a,b</sup>, Johannes Radtke<sup>a,b</sup>, Tim Thomas<sup>a,b</sup>,

<sup>a</sup>*Safetec Entsorgungs- und Sicherheitstechnik GmbH*

<sup>b</sup>*Kurpfalzring 98a, D-69123 Heidelberg, Germany*

<sup>c</sup>*Wittland 44g, D-22589 Hamburg, Germany*

---

## Abstract

Dismantling nuclear power plants entails the production of a large amount of contaminated (or potentially contaminated) waste that must be disposed according to national and international regulations. A large part of the end products needs to be stored in special repositories, but a significant part of it is slightly contaminated or not contaminated at all, making it possible to free release it. One possible approach to free release measurements uses Large Clearance Monitors, chambers surrounded by plastic scintillation detectors that can measure up to 1000kg of waste. Due to the composite nature of the detection system in a Large Clearance Monitor, it is easy to imagine that one can apply 3D imaging algorithms to localize radioactive sources inside a waste package. In this work we will show how a special algorithm that maximizes the conditional informational entropy allows decisions about the clearance of portions of the sample.

*Keywords:* Clearance measurements, Conditional Entropy, nuclear waste imaging

---

## Introduction

One major path for clearance of large amount of waste arising from the decommission of nuclear power plants is based on measurements with Large Clearance Monitors (LCM), devices that utilize multi-detector plastic scintillation arrays (LCMs can consist of up to 24 plastic scintillation detectors) to offer both, extremely low minimum detectable activities (MDA) and short measurement times for waste packages weighing up to one metric ton. LCMs represent in general the most efficient way to measure big and heavy samples. Such clearance measurements are performed also by means germanium detectors (or arrays of germanium detectors) with beam collimators both for waste packages (rotating the sample and measuring its emitted radiation in several different directions) and for whole rooms or buildings (measuring the radiation emitted by the surface of a room by means of a collimated static detector). It has to be pointed out though that germanium detectors are slow and inefficient as each single measurement requires 25-30 minutes and furthermore such devices require delicate cooling systems with liquid nitrogen. In order to handle the large amount of waste produced

during the decommissioning of a nuclear power plant, the measurement for the release procedure must be sufficiently short. For this reason, Large Clearance Monitors (LCM) are used for this task.

However, a major problem with these devices is to obtain reliable information of so-called hotspots, i.e. contaminated or activated material in the waste-package. While the  $4\pi$ -setup of the detectors allows a crude localization of one hotspot (Mirion Technologies RTM644Inc User Manual), no analysis has been conducted so far to test the uncertainty of the estimated activity. Moreover, the localization of hotspots are routinely implemented in a sufficiently high radioactive environment [1, 2] by employing high-purity germanium detectors, but the low radioactivity needed for clearance measurements, presents a different problem. Rather than posing the question where the activity is likely to be located for signals which can be clearly distinguished from the background, for clearance measurements all possible geometrical and hardware uncertainties have to be taken into account for the minimum detection limit and thus the possible activity distributions have to be derived according to ISO 11929. In order to solve the problem of distinguishing the background radiation from the one produced by a sample with a contaminated hotspot, we propose a new method that resembles the imaging techniques used in medical physics.

In this paper we want to present a novel approach

---

\*Corresponding author Tel. +49 (0) 6221 / 65175138

*Email address:* michele.pastena@safetec-hd.de (Michele Pastena)

to the localization and the estimate of radioactivity in contaminated waste packages. The new procedure uses an imaging algorithm to reconstruct accurate images of the radioactivity distribution in a given waste package, allowing fast and reliable decisions for clearance of potentially contaminated or activated material. The proposed method relies on the maximization of informational entropy. This algorithm is used in the medical field for the imaging of tissues in the human body by means of PET/SPECT scans.

In the section 1 we will summarize the most common techniques used to determine the activity of low activated material that can be potentially free released (clearance measurements) mentioning the models and techniques prescribed by the international standards. In the sections from 2 to 4 we will present the Conditional Entropy Maximization, an imaging technique widely used in medical physics and we will show the changes needed to adapt it to the purpose of clearance measurements. In section 5 we will present the mathematical machinery needed to make the aforementioned algorithm compliant with the regulatory norms regarding the determination of the characteristic limits (decision threshold, detection limit and limits of the coverage interval) for measurements of ionizing radiation provided by the international standard. In the final section 6 we will apply the Conditional Entropy Maximization to some simulated samples. This research did not receive any specific grant from funding agencies in the public, commercial, or not-for-profit sectors.

## 1. State of art of the clearance measurements

Usually a LCM consists of a chamber encompassed by a gamma ray detection system distributed over the whole solid angle around the sample, consisting of 24 polyvinyl toluene (PVT)-based large volume plastic scintillation detectors. In order to reduce the background radiation, massive shielding (i.e. 130 mm steel) surrounds the chamber. The activity of the waste is then estimated using a combined measurement of the 24 count rates. This way the LCM can measure up to 1000 kg of waste in one minute. The LCM is also equipped with a conveyor system for the waste packages.

One major drawback of the plastic scintillation detectors used in the LCMs is the poor energy resolution that makes the identification of the radionuclides in the waste almost impossible. This means that gamma spectra cannot be identified, but only the total count in a given time (usually 60 s) is measured for a really wide range of energies. The estimate of the activity depends then on the knowledge of the radionuclide inventory, also known as nuclide vector (NV). Furthermore, the lacking identification of gamma lines does not allow to discriminate between natural radio nuclides and those

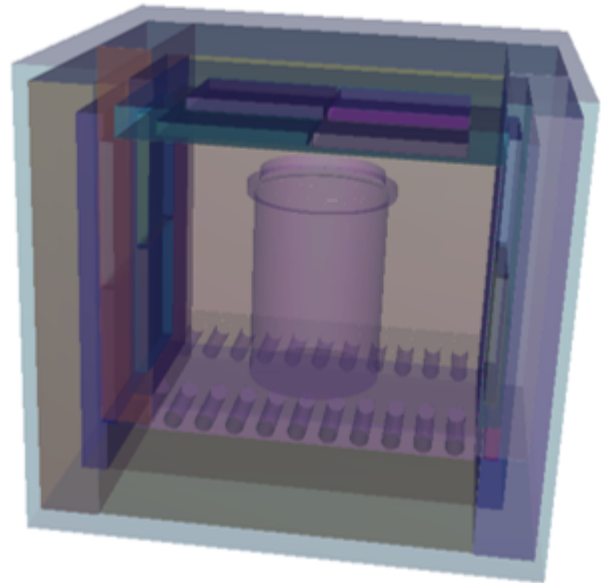


Figure 1: Reproduction of the chamber of a Large Clearance Monitor

produced during the operation of the nuclear power plant.

To obtain the activity of a waste package, the total count rate and a calibration factor  $w$  are needed. The factor  $w = 1/\varepsilon$  is the inverse of the detection efficiency of the whole system (waste and measurement device) i.e. the ability of detecting the photons emitted by the radioactive sources, and depends on the composition of the nuclide inventory. However, the absolute efficiency depends not only on the detection properties of the detector (also known as detector characterization), but is also determined by the waste package, material, and activity distribution (referred to as geometry).

### 1.1. ISO 11929:2019

The aforementioned calibration factor  $w$  is one of the quantities needed to estimate the activity of a waste package. A physical model of the connection between the activity and the other physical observables (count of gamma photons, shielding) is suggested by the international standard ISO 11929 for each type of measurement and environment (high activity, low activity, clearance measurement, etc.). The reason of the importance of this international standard lays on the fact that the law in the field of nuclear safety prescribes the adoption of state-of-art models, techniques and technologies that make the handling of radioactive sources as safe as possible. The duty of the ISO 11929 standard is then to summarize all the most recent and efficient models and prescriptions to be adopted. With reference to the ISO 11929:2019 standard, from now on we will take care exclusively of clearance measurements

(i.e. measurements of samples with such a low activity that they are potentially free releasable). Once we know the calibration factor  $w$  of the measurement device that we are using (both plastic and germanium detectors), the simplified model to evaluate the activity  $a$  is

$$a = (r_g - r_0 \cdot x_3 - x_{41} + x_{42}) w \quad (1)$$

with

- $r_g$  gross count rate measured with the sample in the chamber,
- $r_0$  background count rate measured with empty chamber,
- $x_3$  correction of the background count rate for its variability due to work activities near the device for clearance measurements,
- $x_{41}$  correction for natural radionuclides, i.e.  $^{40}K$  and the  $^{226}Ra$  and  $^{232}Th$  decay series, in the material to be measured,
- $x_{42}$  correction for shielding of the background by the material to be measured.

It has to be remarked that in the present work we will be analyzing only  $^{60}Co$  sources that emit two photons per decay with a probability close to 1. In general it can happen that the nuclide inventory (i.e. the type and relative percentage of radionuclides) is much more complex, requiring more attention in the formulation and solution of the problem. In order to lower the external dose of ionizing radiation, international norms prescribe to fully characterize the activity distribution of a sample (e.g. a waste package) to be analyzed. The core idea is that it is not sufficient that the measurand is below the prescribed threshold, but that we also need a high statistical confidence (typically 95%). This can be achieved either by comparing case by case the whole statistical distribution with the prescribed thresholds or by calculating the characteristic values (in particular the upper limit of the coverage interval and the detection limit). The second option is clearly the most straightforward, and to this end we need the uncertainty and all the statistical characteristic values according to [3]. The uncertainty for the activity (1) is given by

$$u^2(a) = w^2 \left[ \frac{r_g}{t_g} + x_3^2 \frac{r_0}{t_0} + r_0^2 x_3^2 u^2(x_3) + u^2(x_{41}) + u^2(x_{42}) \right] + a^2 u_{rel}^2(w)$$

with  $u_{rel}(w) = u(w)/w$  relative uncertainty of  $w$ . This formula is the starting point to calculate all the characteristic limits of the activity distribution, as it is

explained in Appendix A. Indeed, the uncertainty for an assumed true value  $\tilde{a}$  is then

$$\tilde{u}^2(\tilde{a}) = w^2 \left[ \frac{1}{t_g} \left( \frac{\tilde{a}}{w} + \frac{n_0}{t_0} x_3 + x_{41} + x_{42} \right) + x_3^2 \frac{r_0}{t_0} + r_0^2 \cdot u^2(x_3) + u^2(x_{41}) + u^2(x_{42}) \right] + \tilde{a}^2 u_{rel}^2(w)$$

and thus we can calculate the following characteristic values for the simplified evaluation model:

- decision threshold

$$a^* = k_{1-\alpha} \tilde{u}(0) = k_{1-\alpha} w \left\{ \frac{1}{t_g} \left( \frac{n_0}{t_0} x_3 + x_{41} + x_{42} \right) + x_3^2 \frac{r_0}{t_0} + r_0^2 u^2(x_3) + u^2(x_{41}) + u^2(x_{42}) \right\}^{1/2}$$

where  $k_{1-\alpha}$  is the  $(1-\alpha)$ -quantile of a normal distribution (typically  $\alpha = 0.05$ ),

- detection limit: it is obtained by solving the recursive equation

$$a^\# = a^* + k_{1-\beta} \tilde{u}(a^\#) \quad (2)$$

where  $k_{1-\beta}$  is the  $(1-\beta)$ -quantile of a normal distribution (typically  $\beta = 0.95$ ),

- upper and lower limit of the coverage interval

$$a^\triangleleft = a - k_p u(a) \quad ; \quad a^\triangleright = a + k_q u(a)$$

where  $p = \omega(1-\gamma/2)$ ,  $q = 1-\omega\gamma/2$ , with  $\omega = \Phi(y/u(y))$  probability corresponding to  $y/u(y)$  (assuming that the activity is normally distributed), and  $\gamma = 0.05$ .

These definitions hold in the case of normally distributed activities. In the most general case, we do not need to specify a probability distribution as it is discussed in Appendix A. As it has been pointed out, these values allow us to make decisions about the riskiness of contaminated and nuclear waste in the case of clearance measurements.

## 2. Conditional Entropy Maximization for contaminated waste

In the field of medical physics, reconstructing images of the inner parts of a human body for clinical purposes has always been a challenge. The Single Photon Emission Tomography (SPECT) is mostly used to detect functional or metabolic images of a tissue [4] and has analogies with the characterization of radioactive waste

packages. The core idea of the SPECT in medical physics is to inject a radioactive substance (typically emitting X rays) in living tissues and measure the count rate of photons out of the body along several different directions. This is achieved by encompassing the body in a  $360^\circ$  (in a plane) or a  $4\pi$  (in the space) detection system: this allows the reconstruction of the tissue itself. A similar imaging technique is the Positron Emission Tomography (PET) in which, instead, a positron-electron pair annihilates and emits two photons in opposite directions [5]; in this case the image is reconstructed via measurements of the coincidence count rate. A plethora of imaging algorithms has been proposed [6] in the past decades; here we will focus on the Conditional Entropy Maximization (CEM), in which the image of a radioactive or contaminated source is reconstructed by means of the maximization of the informational entropy.

Entropy maximization is a general technique to solve problems whose analytic solution is not possible or computationally complicated. This approach requires a straightforward and unambiguous definition of the entropy [7, 8]. Entropy maximization overcomes issues of other methods and furthermore allows to bring prior information into the calculation.

The general idea behind the entropy maximization is to define a space  $Y$  of the measured observable  $y \in Y$  (a single quantity or a vector of quantities) and a parameter space  $\Lambda$  of the observable  $\lambda \in \Lambda$  to be estimated. We can then define a probability density function  $P(y; \lambda)$  over the parameter space that is in general difficult to maximize (i.e. we cannot find in general the most likely  $\lambda$  that realizes the observed  $y$ ). Therefore, we introduce a fictitious space  $X$  and a mapping  $x \rightarrow y$ , and thus we move our problem of finding the parameter value (or values) to the problem of maximizing another functional (in this case the conditional entropy) defined on a different space. The task is then to assign an entropy function that is compatible with the prior information about the system and the measurement process, and then maximize it with a constraint given by the outcome of the measurement.

We will now show how this general approach can be applied to the reconstruction of an image by measuring the count of emitted photons (or coincidence counts). The measurement is performed by enclosing the sample in a chamber surrounded by detectors (in a plane or in the space) that can measure the number of emitted photons in different directions (see Fig. 2). The measured count rates  $y_j$  ( $j = 1, \dots, M$  with  $M$  total number of detectors) can be modeled as a Poisson variable and the sample as a matrix of  $N$  pixels (or cells), each with activity  $\lambda_i$ . The goal is thus to properly model the emission and measurement process in order to define the probability (or likelihood) function  $P(y; \lambda)$ . First of all, we can define a matrix  $p_{ij}$  of the ratios between

the intensity detected by detector  $j$  and the decay rate at cell (i.e. pixel)  $i$ . In the following we will refer to these quantities as efficiencies. The mean value of the measured count is then given by

$$\mu_j = t_m \sum_{i=1}^N \lambda_i p_{ij} \quad (3)$$

with  $t_m$  time of the measurement. If we assume the measured counts to be Poisson distributed, then the conditional probability that a realization  $y = (y_1, \dots, y_M)$  of the measurand is obtained given a set of  $\lambda_i$  is the joint distribution of  $M$  Poisson variables

$$P(y|\lambda) = \prod_{j=1}^M \frac{e^{-\mu_j} \mu_j^{y_j}}{y_j!}$$

that takes the following form by inserting the (3)

$$P(y|\lambda) = \prod_{j=1}^M \frac{\exp(-t_m \sum_{i=1}^N \lambda_i p_{ij}) (t_m \sum_{i=1}^N \lambda_i p_{ij})^{y_j}}{y_j!}.$$

The conditional entropy of a measurement  $y \in Y$  given a distribution  $\lambda \in \Lambda$  of the parameter to be estimated is then given by [9, 10, 11]

$$H(y|\lambda) = - \sum_{\lambda} P(\lambda) \left[ \sum_y P(y|\lambda) \log P(y|\lambda) \right] \quad (4)$$

with  $P(\lambda)$  prior distribution function. The conditional entropy (4) measures the information about the knowledge of our system, and the realization  $\hat{\lambda} = (\hat{\lambda}_1, \dots, \hat{\lambda}_N)$  that maximizes (4) is the one most likely to be realized. Following [9], the maximization of  $H(y|\lambda)$  with respect to the parameter (or the set of parameters)  $\lambda$  yields

$$P(y|\hat{\lambda}) \left[ \lambda_i \frac{\partial P}{\partial \lambda_i} \log P(y|\lambda) + \lambda_i t_m P(\lambda_i) (1 + \log P(y|\lambda)) \left( \sum_{j=1}^M \frac{y_j p_{ij}}{\sum_{i=1}^N \lambda_i p_{ij}} \right) - \lambda_i t_m (1 + \log P(y|\lambda)) \sum_{j=1}^M p_{ij} \right]_{\lambda_i = \hat{\lambda}_i} = 0 \quad (5)$$

where  $\hat{\lambda}_i$  are the values of the parameters that maximize the conditional entropy. Equation (5) is verified when

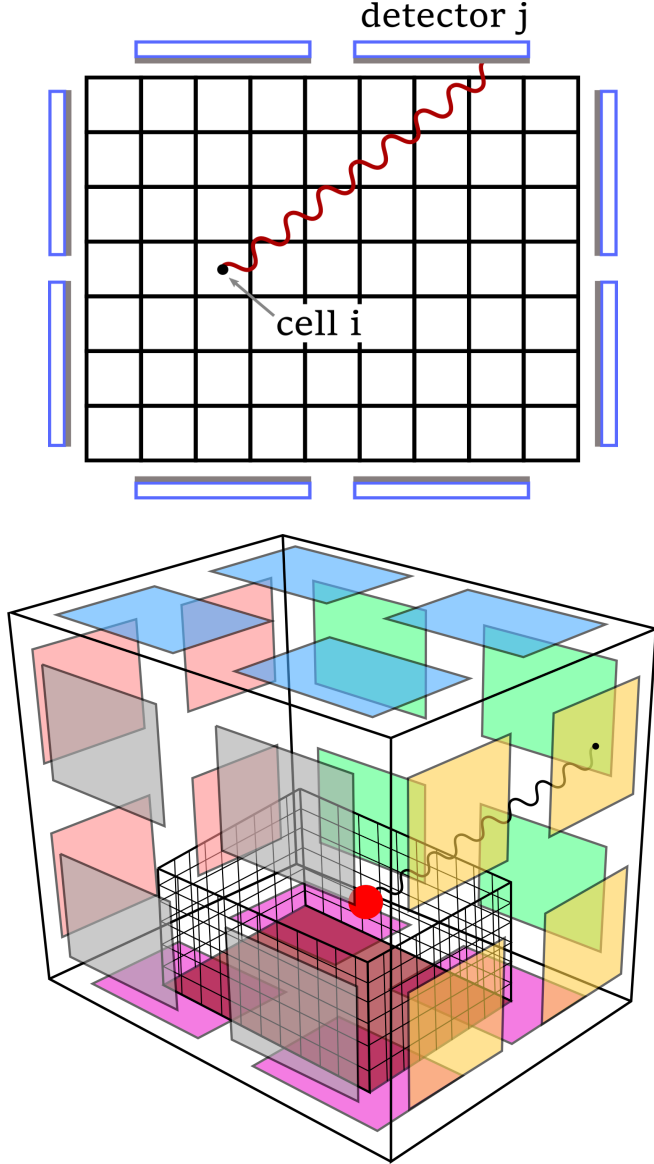


Figure 2: Model of the measurement process and of the sample. In the top picture it is possible to see a section of the sample and of the LCM showing how the emission and detection is modeled in order to properly define the conditional entropy and the detection efficiency. In the bottom picture an illustrative 3D model of the LCM and of the measurement process.

the second factor vanishes ( $P(y|\lambda) \neq 0$ ), leading to

$$\hat{\lambda}_i = \frac{\hat{\lambda}_i}{P(\hat{\lambda}_i) (1 + \log P(y|\hat{\lambda}_i)) t_m \sum_{j=1}^M p_{ij}} \times \left[ \frac{\partial P}{\partial \lambda_i} \Big|_{\lambda_i = \hat{\lambda}_i} \log P(y|\hat{\lambda}_i) + P(\hat{\lambda}_i) (1 + \log P(y|\hat{\lambda}_i)) t_m \sum_{j=1}^M \frac{y_j p_{ij}}{\sum_{i=1}^N \hat{\lambda}_i p_{ij}} \right]. \quad (6)$$

This equation has no closed solution, thus we need to solve it numerically. In particular, given the special form of (6), an iterative solution can be achieved by setting the right-hand-side as the estimate for the  $(k+1)$ -th iterative step of the left-hand-side:

$$\hat{\lambda}_i^{k+1} = \frac{\hat{\lambda}_i^k}{P(\hat{\lambda}_i^k) (1 + \log P(y|\hat{\lambda}_i^k)) t_m \sum_{j=1}^M p_{ij}} \times \left[ \frac{\partial P}{\partial \lambda_i} \Big|_{\lambda_i = \hat{\lambda}_i^k} \log P(y|\hat{\lambda}_i^k) + P(\hat{\lambda}_i^k) (1 + \log P(y|\hat{\lambda}_i^k)) t_m \sum_{j=1}^M \frac{y_j p_{ij}}{\sum_{i=1}^N \hat{\lambda}_i^k p_{ij}} \right]. \quad (7)$$

Considering that  $P(y|\hat{\lambda})$  is a probability (and thus non-negative) and that in a PET or SPECT system it is much smaller than 1, we can then use the approximation  $1 + \log P(y|\hat{\lambda}_i^k) \approx \log P(y|\hat{\lambda}_i^k)$ . This leads to the formula for the estimate of the activity of each pixel of a waste package:

$$\hat{\lambda}_i^{k+1} = \frac{\hat{\lambda}_i^k}{P(\hat{\lambda}_i^k) t_m \sum_{j=1}^M p_{ij}} \times \left[ \frac{\partial P}{\partial \lambda_i} \Big|_{\lambda_i = \hat{\lambda}_i^k} + P(\hat{\lambda}_i^k) t_m \sum_{j=1}^M \frac{y_j p_{ij}}{\sum_{i=1}^N \hat{\lambda}_i^k p_{ij}} \right]. \quad (8)$$

This means that we can estimate the activity and the position of radioactive sources if we choose  $\lambda_i$  to be the activity of pixel  $i$ .

As it is clear from (8), the role of the prior is crucial. What one needs is a function that encompasses all the prior information about the system and the measurement. In our case, we have only considered the case of a uniform prior  $P(\lambda) = const. = 1$ , meaning that we assume to have no prior knowledge: this choice simplifies a lot the formula (8) and reduces our algorithm to the Maximization of the Likelihood function [7, 8]:

$$\hat{\lambda}_i^{k+1} = \frac{\hat{\lambda}_i}{\sum_{j=1}^M p_{ij}} \sum_{j=1}^M \frac{y_j p_{ij}}{\sum_{i=1}^N \hat{\lambda}_i p_{ij}}.$$

Further proposals of priors can be found in [12, 13].

The CEM method provides us a direct way to estimate the position of radioactive sources and their activity. It has to be pointed out that the method explained above is an indirect evaluation model for the activity of a sample (or its portions) since it is necessary to first define a functional (the conditional entropy) over a parameter space and then maximize it to find the most likely physical setting.

### 3. Efficiencies

As it has been shown in section 2, a crucial role is played by the efficiencies  $p_{ij}$ , i.e. the probability that a decay happening at cell (pixel)  $i$  emits a photon that is detected by detector  $j$ . To determine the efficiencies, the following properties of the system are considered:

- the sample (composition, geometry, density, nuclear cross section),
- the detectors (type, position, geometry, tally),
- the relative position of the pixel and the detector and the angle of view,
- the world around the sample and the detectors (the sample carrier, the air between the sample and the detector, the external shielding material, and whatever is not directly either the sample or the detector),
- the source (the isotopic composition, the emission probability and energy of the photons),

Given the large number of parameters, this calculation is highly nontrivial and is practically impossible analytically: it is then necessary to perform Monte Carlo simulations. In the following, we will first describe how Monte Carlo N-particle simulations (MCNP) are used to calculate the energy transported from source inside the sample to one of the detectors. Then we will show how, starting from the properties of the detectors (in our case plastic scintillation detectors), we can transform that into an estimate of the photon count.

The procedure to calculate the efficiencies  $p_{ij}$  is then the following:

1. the sample and the detection are modeled in the framework of MCNP;
2. a standard radioactive source is placed in each cell of the sample;
3. a Monte Carlo simulation of the propagation of gamma photons through the system is performed;
4. the energy deposited on the detectors is converted into a count of detected photons;
5. the efficiency is calculated as the ratio of detected intensity and decay rate.

#### 3.1. MCNP

MCNP<sup>®</sup> is a general-purpose, continuous-energy, generalized-geometry, time-dependent, Monte Carlo radiation-transport code designed to track many particle types over broad ranges of energies [14].

Specific areas of application include, e.g. radiation protection and dosimetry, radiation shielding, radiography, medical physics, nuclear criticality safety, detector design and analysis, nuclear oil well logging, accelerator target design, fission and fusion reactor design, decontamination and decommissioning. The code treats an arbitrary three-dimensional configuration of materials in geometric cells bounded by first- and second-degree surfaces.

The transport is based on point-wise cross-section data. For photons, the code accounts for incoherent and coherent scattering, the possibility of fluorescent emission after photoelectric absorption, absorption in pair production with local emission of annihilation radiation, and bremsstrahlung.

The code provides easy-to-use and very versatile general sources and flexible tallies. In the specific case of the calculation of efficiencies for detectors in a Large Clearance Monitor the sources are modeled by a isotropic point source located in the center of each pixel. The energy distribution of the source photons reflects the decay gamma energies for the respective radio nuclide. The code then transports the particles through the geometry and a pulse-height tally which records the energy deposited in the detector volume by each primary particle and its secondary particles. The spectrum of the deposited energies is calculated on a very fine resolution ( $\sim 3000$  bins) between 0 eV and 3 keV.

#### 3.2. SimPS

SimPS (Simulated Plastic Scintillator) is a software for plastic scintillation detectors to calculate detection probabilities of photons with specific energies which interact with the detector. Moreover, it takes into account the emission probability, i.e. the number of photons emitted per decay of the radioactive source. In order to do so, a detector characterization and calibration needs to be performed by estimating the energy dependence of the detection probability. This probability is mainly influenced by the discriminator voltage of the detector and can be modeled by means of a cumulative distribution function of a Pareto-distribution (9) whose parameters  $x_m$  and  $\alpha$  are estimated by fitting calibration measurements

$$F(x) = \begin{cases} 1 - \frac{x_m^\alpha}{x^\alpha}, & x \geq x_m \\ 0, & x < x_m \end{cases}. \quad (9)$$

Using this detector characterization and the energy deposition spectrum calculated by MCNP for each detector-pixel pair, it is possible to estimate the efficiencies  $p_{ij}$  used in the CEM algorithm.

#### 4. Application of the CEM to clearance measurements

##### 4.1. Compliance with the ISO 11929

As it has been already pointed out, the analysis of a potentially contaminated sample is subject to the compliance with the international guidelines set by ISO and adopted by the national governments [15]. As it has been reported in section 1.1, the idea behind the standard is that not only the best estimate of the activity is needed to make a decision about a sample, but also its distribution has to be fully characterized by calculating all the statistical characteristic values, i.e. the coverage interval, the detection limit and the decision threshold. In order to achieve this for each measured sample, we need an evaluation model to estimate the activity and its uncertainty once we have performed the measurements as it has been already explained.

It is then crucial to show if and how the method described in the previous section is able to estimate activity values and their uncertainty. The norm prescribes to use an algebraic model for the answer to this question, and thus it might seem that the CEM method is not compliant with the ISO 11929:2019. In fact, the CEM method is not only an imaging technique, but also a way to estimate the activity (and the respective uncertainty) of any portion of a sample, making it suitable to our purpose.

Looking back at the general formulation of the CEM method, we can fix the general parameter  $\lambda$  to be the activity of a cell of the sample and this allows the CEM to produce an estimate of the activity of each cell: this is a good result, but still incomplete as the CEM itself provides no direct method to characterize the distribution of the activity. We will address this problem in the following section 5; for now it is enough to know that the CEM algorithm can be opportunely integrated to fully characterize the activity distribution of each cell of a measured sample. This puts us in the condition to be compliant with the ISO 11929:2019, since we have both a model of evaluation of the activity (resp. activities of the single cells or portions of the sample) and an estimate of the uncertainty (resp. uncertainty for each cell or portions of the sample). In the following section 4.2 we will show our proposal to calculate all the characteristic values of the activity distribution for single cells and for whatever portion of the sample, showing also that this improves a lot the limits of the coverage interval of the activity of the whole sample.

##### 4.2. Application of the CEM to the clearance of waste packages

The general CEM method presented in section 2 has a direct and easy application for PET imaging systems. Despite the application to SPECT systems is straightforward as well, there are some technical difficulties that make it tricky. In fact, in a PET system, given the nature of the emission process, the device measures coincidence count rates and thus can directly measure the net count rate of pair annihilations. On the other hand, in a SPECT system (as it is in our case), the detectors measure also the background radiation (due to natural radioactive sources) and thus one can either subtract the background from the gross count rate, or slightly change the formula (8) in order to use the gross count rate instead. Using the gross count rate is of help because in our case the count due to the sample can be similar or even lower than the count of background photons. Moreover, using the gross count rate will make also the calculation of the uncertainties easier, as it will be shown in the following. The most straightforward way of circumventing the problem is to substitute the mean count (3) with the corresponding expression of the gross number of emitted photons according to the evaluation model (1) of the ISO 11929:2019

$$\mu_j = t_m \sum_{i=1}^N \lambda_i p_{ij} \longrightarrow t_m \left( x_3 r_{0,j} - x_{42} + \sum_{i=1}^N \lambda_i p_{ij} \right). \quad (10)$$

This modifies the formula (6) leading to

$$\hat{\lambda}_i = \frac{\hat{\lambda}_i}{P(\hat{\lambda}_i) (1 + \log P(y|\lambda_i)) t_m \sum_{j=1}^M p_{ij}} \left[ \begin{aligned} & \left[ \frac{\partial P}{\partial \lambda_i} \right]_{\lambda_i = \hat{\lambda}_i} \log P(y|\hat{\lambda}_i) + \\ & + P(\hat{\lambda}_i) (1 + \log P(y|\hat{\lambda}_i)) t_m \\ & \times \sum_{j=1}^M \frac{y_j p_{ij}}{r_{0,j} x_3 - x_{42} + \sum_{i=1}^N \hat{\lambda}_i p_{ij}} \end{aligned} \right]$$

where  $y = (y_1, \dots, y_N)$  are now the gross count rates of the  $N$  detectors. It has to be pointed out that the substitution (10) is also needed to calculate the characteristic statistical limits of the activity distribution as it will be shown in the next section. The recursive formula (8) for the estimate of the activity becomes then

$$\hat{\lambda}_i^{k+1} = \frac{\hat{\lambda}_i^k}{P(\hat{\lambda}_i^k) t_m \sum_{j=1}^M p_{ij}} \left[ \begin{aligned} & \left[ \frac{\partial P}{\partial \lambda_i} \right]_{\lambda_i = \hat{\lambda}_i^k} \\ & + P(\hat{\lambda}_i^k) t_m \sum_{j=1}^M \frac{y_j p_{ij}}{r_{0,j} x_3 - x_{42} + \sum_{i=1}^N \hat{\lambda}_i^k p_{ij}} \end{aligned} \right]. \quad (11)$$

As a direct consequence, also the maximum likelihood formula (i.e. with constant prior) is modified:

$$\hat{\lambda}_i^{k+1} = \frac{\hat{\lambda}_i^k}{\sum_{j=1}^M p_{ij}} \sum_{j=1}^M \frac{y_j p_{ij}}{r_{0,j} x_3 - x_{42} + \sum_{i=1}^N \hat{\lambda}_i^k p_{ij}}.$$

## 5. Calculation of the characteristic limits

The first step to calculate the characteristic statistical limits of the activity distribution is to estimate the uncertainty of the activities calculated by means of the CEM algorithm. As we have already pointed out, the CEM algorithm itself does not provide a direct way to estimate the uncertainty, but this problem can be easily circumvented by propagating the uncertainty of the measurement and of any other input parameter (according to their statistical distribution). The measured values  $y_i$  are count rates of photons, and thus they are Poisson distributed. The idea is then to generate  $P$  Poisson random sets of data  $y^\eta = (y_1^\eta, \dots, y_M^\eta)$ ,  $\eta = 1, \dots, P$  (or repeating the measurement  $P$  times) and perform the CEM calculation for each of this randomly generated (or measured) set of data. This will provide  $P$  different activity distributions  $\lambda^\eta = (\lambda_1^\eta, \dots, \lambda_n^\eta)$  and then we can use the obtained values to calculate the activity and the uncertainty for each portion of the sample (in the most simple case for each single cell) as the arithmetic mean and the standard deviation of the values produced by the CEM algorithm:

$$\lambda_i = \frac{1}{P} \sum_{\eta=1}^P \lambda_i^\eta \quad (12)$$

$$u_i^2(\lambda_i) = \frac{1}{P-1} \sum_{\eta=1}^P (\lambda_i^\eta - \lambda_i)^2. \quad (13)$$

This procedure can be repeated if we have any other known source of uncertainty for our count rates. In particular, looking at (11), it is necessary to propagate also the uncertainty of the background  $r_0$ , of the efficiencies  $p_{ij}$  (that are normally distributed), of the factor  $x_3$  and of the shielding  $x_{42}$ .

Each cell will then have a distribution of estimated activities  $(\lambda_i^1, \dots, \lambda_i^P)$  that we can sort such that  $\lambda_i^\eta \leq \lambda_i^{\eta+1}$ . Then we can assign to each value  $\lambda_i^\eta$  a cumulative probability  $\eta/P$  and build a discrete cumulative distribution  $F(\lambda_i|y^\eta)$ .

We now have all the ingredients to fully characterize the statistical activity distributions of each portion of the sample. This can be done by following the guidelines of the ISO 11929:2019, i.e. by estimating the uncertainty for specific values of the assumed true value. We need then to calculate the outcome of a measurement  $\tilde{y}_j$  when

the activities  $\lambda_i$  assume some special values  $\tilde{\lambda}_i$ . This can be done following (10):

$$\tilde{y}_j = x_3 r_{0,j} - x_{42} + \sum_{i=1}^N \tilde{\lambda}_i p_{ij}.$$

Then the  $\tilde{y}_j$  have to be varied around the mean and given as input to the CEM formula (11) to estimate the characteristic limits pixel by pixel

$$\hat{\lambda}_i^{k+1} = \frac{\hat{\lambda}_i^k}{P(\hat{\lambda}_i^k) t_m \sum_{j=1}^M p_{ij}} \left[ \left. \frac{\partial P}{\partial \lambda_i} \right|_{\lambda_i = \hat{\lambda}_i^k} \right. \quad (14)$$

$$\left. + P(\hat{\lambda}_i^k) t_m \sum_{j=1}^M \frac{(x_3 r_{0,j} - x_{42} + \sum_{i=1}^N \tilde{\lambda}_i p_{ij}) p_{ij}}{r_{0,j} x_3 - x_{42} + \sum_{i=1}^N \hat{\lambda}_i^k p_{ij}} \right].$$

The mean and the standard deviation are then calculated using (12) and (13).

Formula (14) can be seen as the bridge between the CEM algorithm (i.e. the evaluation model for all the cells) and the statistical characteristic limits (for single cells or blocks). In the following we will indeed address the problem not only for single cells, but also for blocks, that can be reduced to single-cell-blocks. To this end we can split the sample itself into two parts  $B_1$  (the part of interest, of which we want to calculate a characteristic limit) and  $B_2$  (the rest), such that we can split the sum  $\sum_{i=1}^N \lambda_i p_{ij}$  in (14) into two parts as follows

$$\sum_{i=1}^N \lambda_i p_{ij} = \sum_{i \in B_1} \lambda_i p_{ij} + \sum_{i \in B_2} \lambda_i p_{ij}$$

where a block can consist even of one single cell or all the cells. In order to keep the pattern of the estimated activity distribution fixed in  $B_1$  and  $B_2$  respectively while varying the assumed true value we define the specific efficiency for the two blocks

$$p_{B_1,j} = \frac{\sum_{i \in B_1} \lambda_i p_{ij}}{\sum_{i \in B_1} \lambda_i} \quad ; \quad p_{B_2,j} = \frac{\sum_{i \in B_2} \lambda_i p_{ij}}{\sum_{i \in B_2} \lambda_i}.$$

With these constrains the iterative CEM formula for the activity in  $B_1$  can be written as follows

$$\hat{\lambda}_{B_1}^{k+1} = \frac{\hat{\lambda}_{B_1}^k}{P(\hat{\lambda}_{B_1}^k) t_m \sum_{j=1}^M p_{B_1,j}} \times \left[ \left. \frac{\partial P}{\partial \lambda_{B_1}} \right|_{\lambda_{B_1} = \hat{\lambda}_{B_1}^k} + P(\hat{\lambda}_{B_1}^k) t_m \right.$$

$$\left. \times \sum_{j=1}^M \frac{(x_3 r_{0,j} - x_{42} + \tilde{\lambda}_{B_1} p_{B_1,j} + \tilde{\lambda}_{B_2} p_{B_2,j}) p_{B_1,j}}{r_{0,j} x_3 - x_{42} + \tilde{\lambda}_{B_2} p_{B_2,j} + \hat{\lambda}_{B_1}^k p_{B_1,j}} \right]. \quad (15)$$



Assuming a true value for  $\tilde{\lambda}_{B_1}$ , we can then sample the input parameters and estimate the characteristic values. It has to be remarked that the numerator and the denominator of (15) have to be sampled separately as they represent measurements of the background that happen respectively with (numerator) and without (denominator) the sample (i.e. the block of interest) in the chamber.

### 5.1. Decision threshold

Following the prescriptions of the ISO 11929:2019, if we want to calculate the decision threshold of the activity of a sample, we need to estimate the uncertainty of a vanishing true value of the activity. The decision threshold can be defined as the minimum value that can be distinguished from the background with a given confidence and in this case the definition of background itself is crucial. In order to calculate the decision threshold for a block of pixels (or eventually for a single pixel), we need to consider the radiation emitted by the rest of the sample as part of the background.

In order to calculate the decision threshold for  $B_1$ , we need to set its total activity  $\tilde{\lambda}_{B_1} = 0$  while the activities of the cells in  $B_2$  are left unchanged (i.e. the value estimated by the CEM) and are taken into account as part of the background radiation. This can be obtained only by setting all the  $\tilde{\lambda}_i$  in  $B_1$  to zero (since activities are non negative), leading to the following iterative formula for the decision threshold  $\lambda_{B_1}^*$  of block  $B_1$  that follows from (15)

$$\hat{\lambda}_{B_1}^{k+1} = \frac{\hat{\lambda}_{B_1}^k}{P\left(\hat{\lambda}_{B_1}^k\right) t_m \sum_{j=1}^M p_{B_1,j}} \left[ \frac{\partial P}{\partial \lambda_{B_1}} \Big|_{\lambda_{B_1} = \hat{\lambda}_{B_1}^k} + P\left(\hat{\lambda}_{B_1}^k\right) t_m \sum_{j=1}^M \frac{\left(x_3 r_{0,j} - x_{42} + \tilde{\lambda}_{B_2} p_{B_2,j}\right) p_{B_1,j}}{r_{0,j} x_3 - x_{42} + \tilde{\lambda}_{B_2} p_{B_2,j} + \hat{\lambda}_{B_1}^k p_{B_1,j}} \right].$$

By sampling the input parameters of this formula around the fixed true values  $(r_0, x_3, x_{42}, \tilde{\lambda}_{B_2}, p_{B_1,j}, p_{B_2,j})$ , we get many values of  $\lambda_{B_1}^n$  that are distributed according to  $F(\tilde{\lambda}_{B_1} = 0 | y^n)$  as described in the previous paragraph. The  $(1 - \alpha)$ -quantile (typically with  $\alpha = 0.05$ ) of this distribution is the decision threshold  $\lambda_{B_1}^*$ .

### 5.2. Detection limit

The detection limit  $\lambda_{B_1}^\#$  of  $B_1$  is the smallest true value of the activity in the block, for which the probability of a false negative (as it is explained in section Appendix A) does not exceed the specified probability  $\beta$  (typically 0.05).

By applying the iterative formula (15), the detection limit  $\lambda_{B_1}^\#$  is the value of  $\tilde{\lambda}_{B_1}$  for which the  $\beta$ -quantile

of the distribution function  $F(\tilde{\lambda}_{B_1} | y^n)$  is equal to the decision threshold. This value can be calculated iteratively by applying root-finding methods.

### 5.3. Limits of the coverage interval

The limits of the coverage interval  $(\lambda_{B_1}^\triangleleft, \lambda_{B_1}^\triangleright)$  are defined in such a way that the coverage interval contains the true value of the measurand within the specified probability  $1 - \gamma$  (typically with  $\gamma = 0.05$ ). In the following we use the definition of the probabilistic symmetric coverage interval which defines the limits of the coverage interval as the  $\gamma/2$ -quantile  $(\lambda_{B_1}^\triangleleft)$  and  $(1 - \gamma/2)$ -quantile  $(\lambda_{B_1}^\triangleright)$  of the distribution function  $F(\lambda_{B_1} | y^n)$ .

## 6. Examples

In the following we will show the accuracy of the proposed method by simulating measurements with MCNP and reconstructing the sources by means of the CEM method. The two examples that follow will summarize all the things that have been discussed so far and will show that the method presented is safe and reliable enough to handle waste packages from nuclear facilities.

The first simulated sample is an iron block of size 120 x 80 x 23.5 cm (x, y and z dimension) and density 1.681 g/cm<sup>3</sup> carried by a steel sample-carrier-box and an aluminum pallet. A point source of <sup>60</sup>Co of activity 5 kBq is placed right in the middle of the sample as it is shown in Fig. 3 while the CEM-reconstructed distribution is in Fig. 4. For the reconstruction, we have sampled the input parameters 10000 times around the measured (or in this case simulated) values according to their statistical distribution. For each sampled set of data, the recursive CEM formula (11) has been used with  $k = 10^4$  to guarantee that the calculations have satisfactorily converged. The activity for each pixel is then calculated as the arithmetic mean of all the 10000 runs of the algorithm. The characteristic values have been calculated according to the prescriptions layed out in the previous section. For the whole sample, the total activity is  $\lambda_{tot} = 4890$  Bq with a standard deviation of  $\sigma_{tot} = 116$  Bq. The lower and upper limit of the 95% symmetric coverage interval are  $\lambda_{tot}^\triangleleft = 4695$  Bq and  $\lambda_{tot}^\triangleright = 5077$  Bq. The decision threshold is  $\lambda_{tot}^* = 60$  Bq and the detection limit  $\lambda_{tot}^\# = 124$  Bq. The integral efficiency of the whole detection system is 21.2% for that activity distribution. The characteristic values of this sample are summarized in Table 1.

The second simulated sample consists of the same iron block, with two <sup>60</sup>Co point sources of 5 kBq each, located at the top "right" and at the bottom "left" (from the view of the experimenter) corners (see Fig. 5). In Fig.

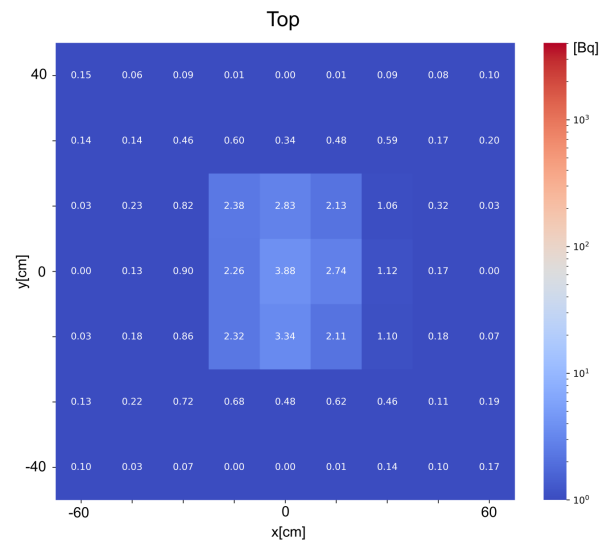
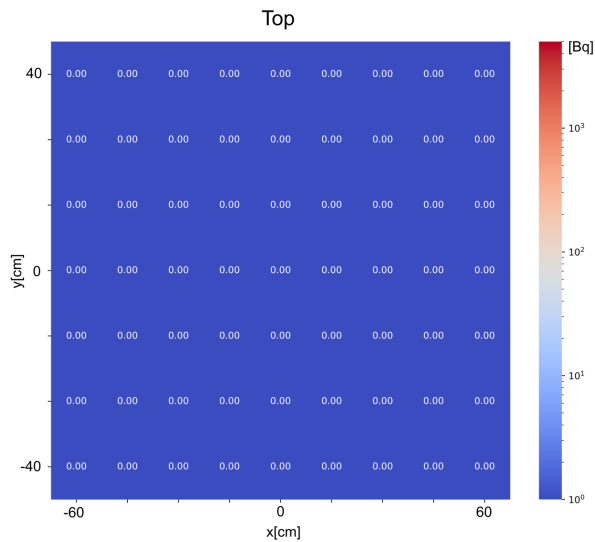
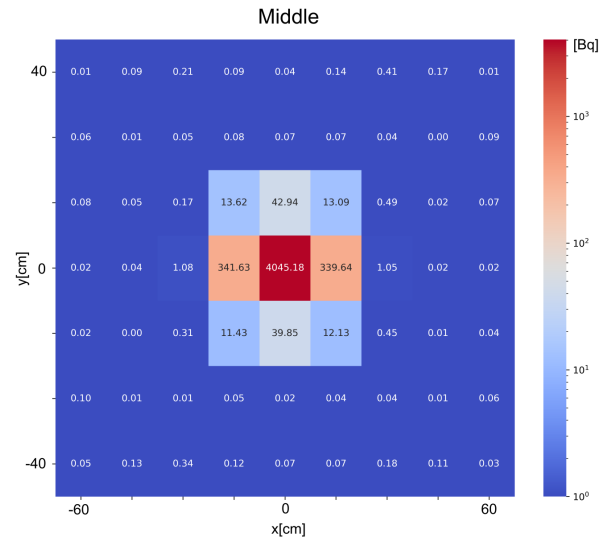
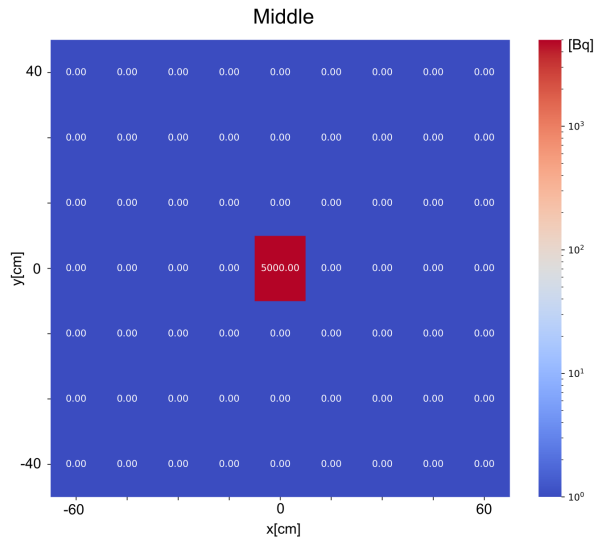
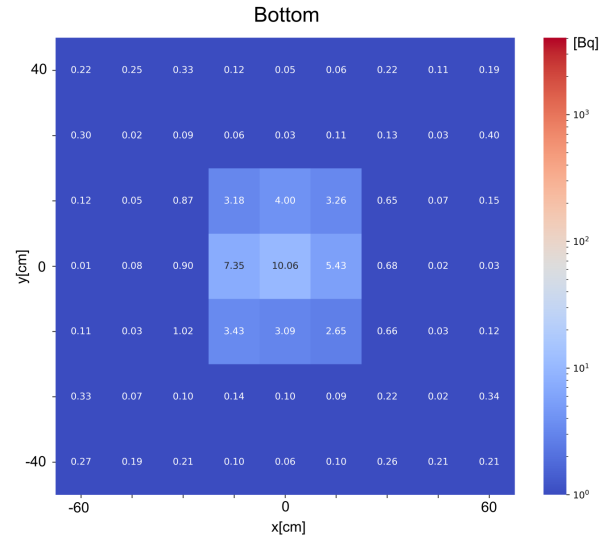
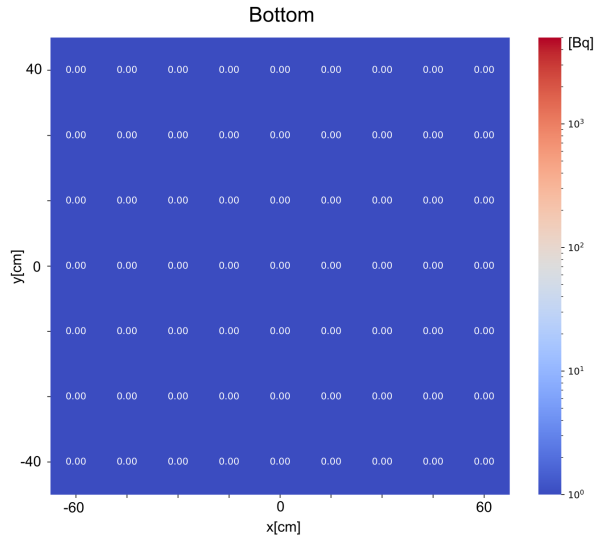


Figure 3: Simulated sample n.1. Uniform iron block of density  $1.681 \text{ g/cm}^3$  with one simulated  $^{60}\text{Co}$  source in the middle of activity  $5 \text{ kBq}$ . The three plots represent the three layers of the sample from bottom to top.

Figure 4: Simulated sample n.1. This figure shows the CEM-reconstructed activity distribution of the sample shown in Fig. 3

	Total
Activity (Bq)	4890
Uncertainty (Bq)	116
Lower limit of coverage (Bq)	4695
Upper limit of coverage (Bq)	5077
Decision threshold (Bq)	60
Detection limit (Bq)	124
Efficiency (%)	21.2

Table 1: Table with all the characteristic values of the simulated sample n. 1 (activity distribution of Fig. 3)

6, the reconstructed activity distribution is shown. As before the same number of data sets (10000) and CEM iteration steps ( $k = 10^4$ ) were used for the calculation and the values shown are the arithmetic means for each pixel. For the whole sample, the total estimated activity is  $\lambda_{tot} = 9954 Bq$  with a standard deviation of  $\sigma_{tot} = 163 Bq$ . The lower and upper limit of the 95% symmetric coverage interval interval are  $\lambda_{tot}^{\downarrow} = 9706 Bq$  and  $\lambda_{tot}^{\uparrow} = 10241 Bq$ . The decision threshold is  $\lambda_{tot}^* = 42 Bq$  and the detection limit  $\lambda_{tot}^{\#} = 90 Bq$ . The integral efficiency over all detectors was calculated to be 31.6% for that activity distribution. The characteristic values of this sample are summarized in Table 2.

The sample was split into two blocks (as in Fig. 7 where they are marked in red and green) which were analyzed separately. The activity in Block 1 (red) is located in the bottom of the sample whereas the activity in Block 2 (green) is located in the top. Due to the fact that the lower source is better shielded (conveyor belt, aluminum pallet, sample carrier box), the block containing this source will clearly have a lower detection efficiency: indeed it has a total efficiency of 27.1% while the other block has an efficiency of 36.4%. Due to the difference in efficiency for block 1 and 2, the decision thresholds were estimated to be respectively  $\lambda_1^* = 71 Bq$  and  $\lambda_2^* = 64 Bq$ . These two values are larger than the decision threshold for the whole sample due to the fact that, when calculating the characteristic limits for a block, the radiation generated by the other one needs to be considered as part of the background. The detection limits are  $\lambda_1^{\#} = 163 Bq$  and  $\lambda_2^{\#} = 150 Bq$ . The mean activity in block 1 was calculated to be  $\lambda_1 = 5124 Bq$  with a standard deviation of  $\sigma_1 = 284 Bq$ , whereas the for block 2 a mean of  $\lambda_2 = 4830 Bq$  and standard deviation of  $\sigma_2 = 241 Bq$  was estimated. The coverage intervals and all other values are summarized in Table 2.

A convergence study of the CEM has also been performed. If we consider the  $(k + 1)$ -th step of the iterative CEM calculation of formula (11), we can define the deviation of cell  $i$  from the previous iterative step

$$\Lambda_i^k = \left| \frac{\lambda_i^{k+1} - \lambda_i^k}{\lambda_i^k} \right|.$$

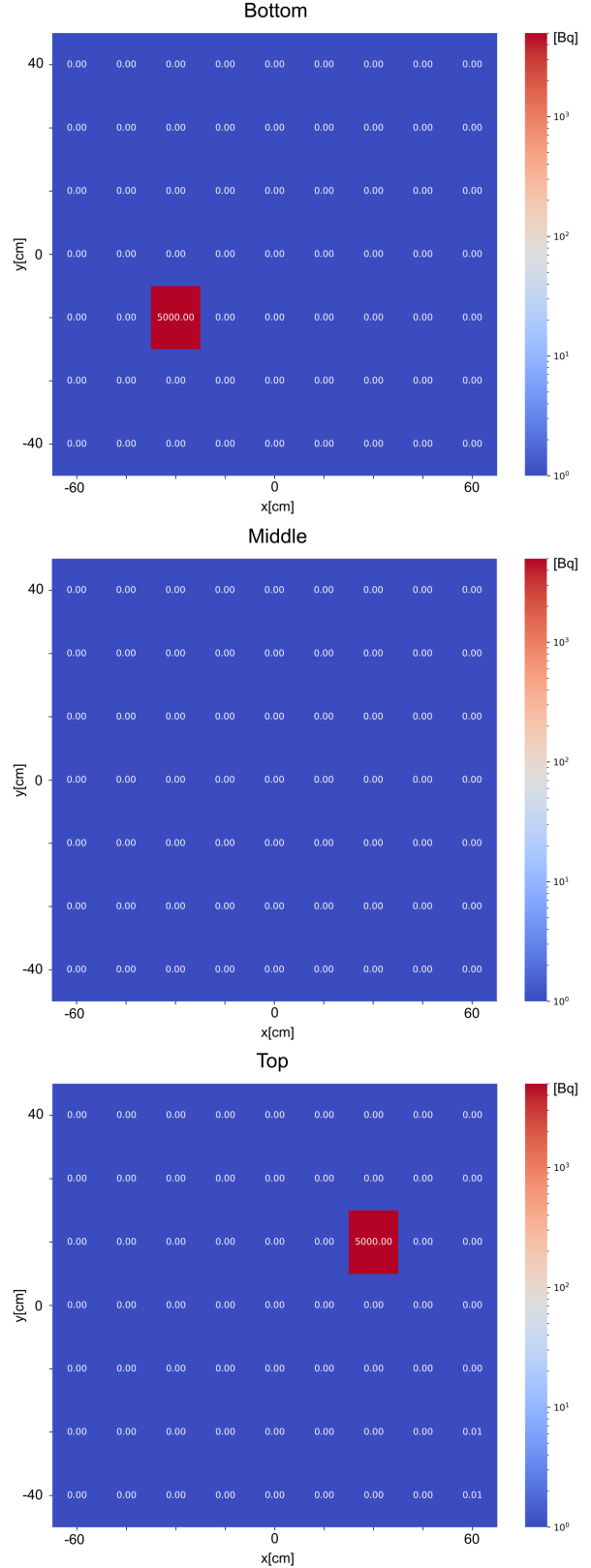


Figure 5: Simulated sample n.2. Uniform iron block of density  $1.681 g/cm^3$  with two simulated  $^{60}Co$  sources of activity  $5 kBq$  each. The three plots represent the three layers of the sample from bottom to top.

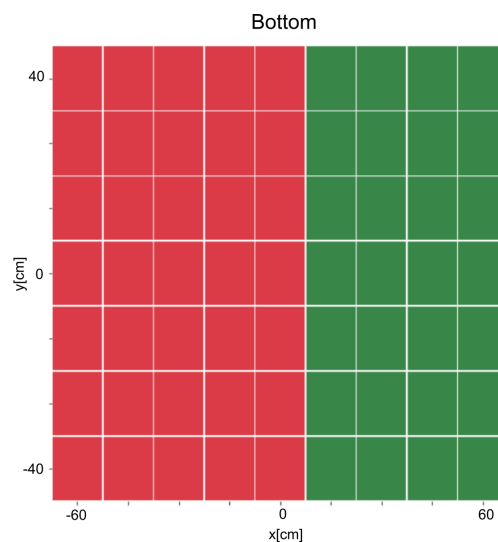
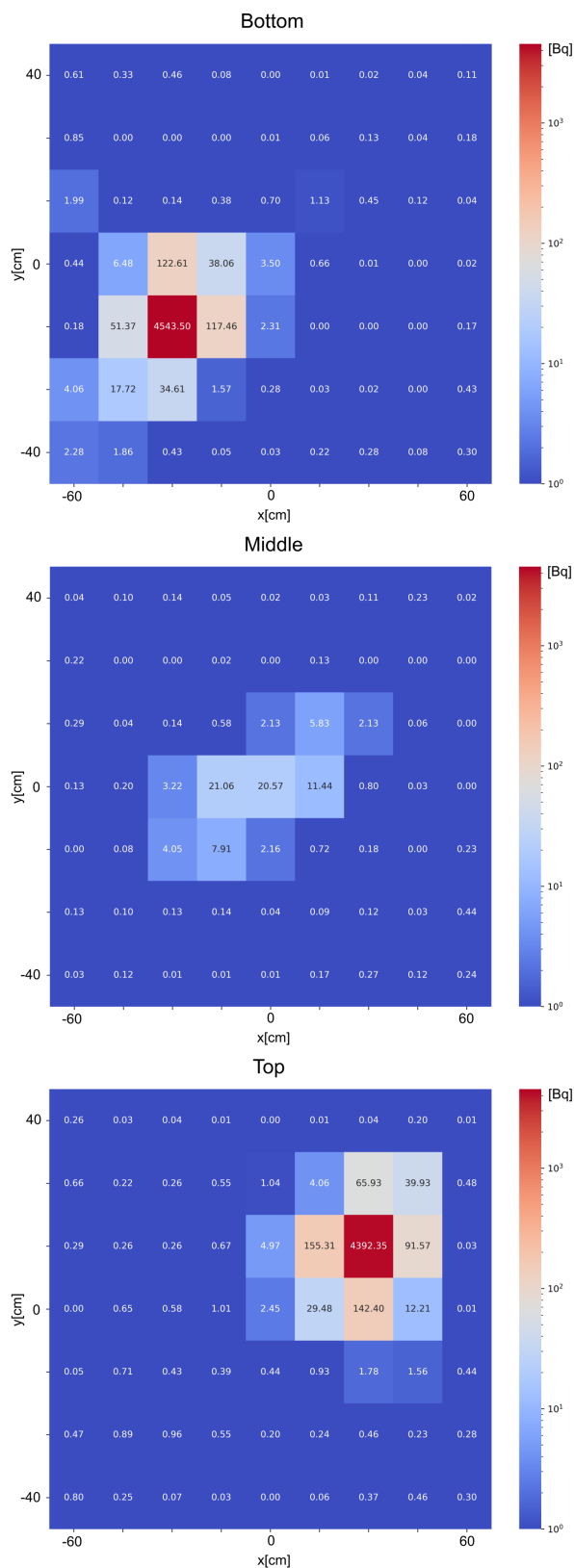


Figure 7: Splitting of sample n.2. Each of the three layers are split equally. The two blocks (red and green) are such that they have approximately the same number of cells

	Total	Block 1	Block 2
Activity (Bq)	9954	5124	4830
Uncertainty (Bq)	163	284	241
Lower limit of coverage (Bq)	9706	4743	4383
Upper limit of coverage (Bq)	10241	5668	5159
Decision threshold (Bq)	42	71	64
Detection limit (Bq)	90	163	150
Efficiency (%)	31.6	27.1	36.4

Table 2: Table with all the characteristic values of the simulated sample n. 2 (activity distribution of Fig. 5)

Figure 6: Simulated sample n.2. This figure shows the CEM-reconstructed activity distribution of the sample shown in Fig. 5

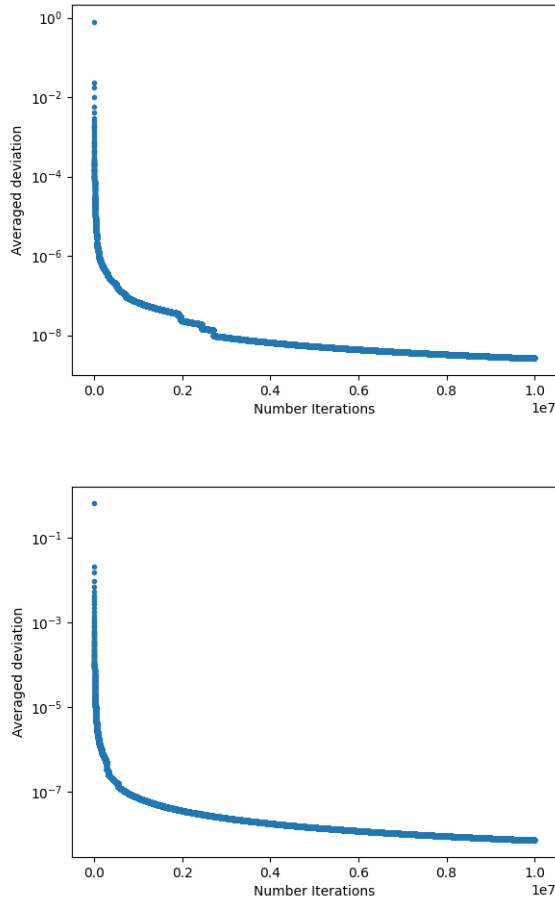


Figure 8: Plot in logarithmic scale of the average deviation as a function of the iterative step  $k$ . The first picture on top shows the plot for a single point source in the middle of the sample (as in Fig. 3); the second pictures shows the plot for two point sources placed at opposite corners of the sample as in Fig. 5

If we average this quantity over all the cells, we have an indicator

$$\Sigma^k = \frac{1}{N} \sum_{i=1}^N \Lambda_i^k$$

of how much the algorithm has converged. In Fig. 8 we have plotted  $\Sigma^k$  for the two cases of a point source in the middle (as in Fig. 3) and of two point sources in opposite corners (as in Fig. 5).

## Conclusion

In this paper we have presented an innovative approach to clearance measurements of waste packages from nuclear facilities. The new procedure, borrowed from medical physics, does not adopt algebraic evaluation models for the estimate of the activity and goes one step further: the maximization of the conditional entropy functional allows the estimate of the activity distribution,

cell by cell (as it happens for the image reconstruction). The presented CEM method can be also adapted to the international ISO 11929 standards by properly defining the characteristic limits for the measured activities. Moreover, it allows to lower the characteristic limits for the free release of the contaminated waste, e.g. by splitting the sample in two or more parts: if a non-releasable sample containing radioactive hotspots can be split into portions whose hotspots do not exceed the legal thresholds separately, then we have achieved the goal of reducing the amount of waste that needs to be stored in special repositories with consequent saving of money and resources.

In this first study, we have then shown that the CEM method reconstructs faithfully the radioactive distribution of a simulated metal block with respectively one and two point sources. The calculation of the characteristic limits of the whole block and of parts of the block shows that we can significantly increase the amount of releasable waste e.g. by splitting the sample. It was shown that the calculated activity matches very well the original activity, easily within the coverage interval. Furthermore, the localization and magnitude of the activity was found to be in good agreement with the activity placed in the sample both for a single hotspot and for two hotspots. The described procedure to calculate characteristic limits provided reasonable estimates of the decision threshold, of the detection limit as well as of the coverage intervals for both the whole sample and for parts of it. It was shown that the characteristic limits strongly depend on the activity distribution, making clear the advantage of this approach. Also we have found that the recursive algorithm requires a finite number of iterations to converge within a given accuracy.

Further studies will include a quantitative analysis of the agreement of the reconstructed image with the original sample, as well as a general rule to fix the number of iterations needed to converge significantly. Moreover we will report the results and conduct further analysis of real samples. Another future extension of the method will include techniques to improve the spatial resolution.

## Acknowledgment

We are thankful to prof. Rolf Michel for supporting our work and encouraging the writing of the present paper.

## References

- [1] G. Amoyal, V. Schoepff, F. Carrel, M. Michel, N. Blanc de Lanaute, J. C. Angélique, Development of a hybrid gamma camera based on timepix3 for nuclear industry applications, Nucl. Inst. and Meth.

- in Phys. Res. Sec. A In Press, Journal Pre-proof (2020).
- [2] M. Duerr, K. Krycki, B. Hansmann, T. Hansmann, A. Havenith, M. Fritzsche, D. Pasler, T. Hartmann, Advanced sectorial gamma scanning for the radiological characterization of radioactive waste packages, *Atw. Internat. Zeitsch. fuer Kernen*. 64 (3) (2019) 160.
- [3] Evaluation of measurement data - guide to the expression of uncertainty in measurement. s.l., BIPM, IEC, IFCC, ILAC, ISO, IUPAC, IUPAP and OIML JCGM 100 (2008).
- [4] Y.-M. Zhu, S. M. Cochoff, Likelihood maximization approach to image registration, *IEEE Trans. Im. Proc.* 11 (12) (2002) p. 1417. doi:10.1109/TIP.2002.806240.
- [5] A. C. Kak, M. Slaney, Principles of Computerized Tomographic Imaging, 2001.
- [6] J. B. A. Maintz, M. A. Viergever, A survey of medical image registration, *Med. Image Anal.* 2 (1) (1998) p. 1. doi:10.1016/S1361-8415(01)80026-8.
- [7] B. R. Frieden, Restoring with maximum likelihood and maximum entropy, *J. Opt. Soc. Am.* 62 (1972) p. 511. doi:10.1364/JOSA.62.000511.
- [8] B. R. Frieden, D. C. Wells, Restoring with maximum entropy: Poisson sources and backgrounds, *J. Opt.Soc. Am.* 68 (1) (1978) p. 93. doi:10.1364/JOSA.68.000093.
- [9] P. P. Mondal, K. Rajan, Image reconstruction by conditional entropy maximisation for pet system, *IEEE Proc. Vis. Im. Sign. Proc.* 151 (5) (2004) p. 345. doi:10.1049/ip-vis:20040717.
- [10] C. L. Byrne, Likelihood maximization for list-mode emission tomographic image reconstruction, *IEEE Trans. Med. Imaging* 20 (10) (2001) 1084. doi:10.1109/42.959305.
- [11] C. L. Byrne, Iterative image reconstruction algorithms based on crossentropy minimization, *IEEE Trans. Image Process* 2 (1) (1993) 96. doi:10.1109/83.210869.
- [12] H. Zhu, H. Shu, J. Zhou, X. Dai, L. Luo, Conditional entropy maximization for pet image reconstruction using adaptive mesh model, *Comp. Med. Im. and Gr.* 31 (2007) p. 166. doi:10.1016/j.compmedimag.2007.01.001.
- [13] A. Lopez, R. Molina, A. K. Katsaggelos, Spect image reconstruction using compound models, 2001 IEEE Int. Conf. Ac. Proc. (2001) p. 1909doi:10.1109/ICASSP.2001.941318.
- [14] C. J. Werner, J. S. Bull, C. J. Solomon, F. B. Brown, G. W. McKinney, M. E. Rising, D. A. Dixon, R. L. Martz, H. G. Hughes, L. J. Cox, A. J. Zukaitis, J. C. Armstrong, R. A. Forster, L. Casswell, Mcnp version 6.2 release notes (2 2018). doi:10.2172/1419730.
- [15] Iso 11929:2019: Determination of characteristic limits (decision threshold, detection limit, and limits of the confidence interval) for measurements of ionizing radiation - fundamentals and applications, International Organization for Standardization, Geneva (2019).
- [16] K. Weise, G. Kanisch, R. Michel, M. Schläger, D. Schrammel, M. Täschner, Characteristic values in measurement of ionizing radiation - material for a critical discussion on fundamentals and alternatives, *Fachver. Str. AK Sigma* 167 (2013).

## Appendix A. Definitions of the characteristic values

The formulae in section 1.1 refer to the calculation of characteristic values in case of a specific evaluation model and under the assumption of a symmetric probability distribution of the measurands. There are some cases though in which these assumptions don't hold or it is even analytically impossible to determine the probability distribution function and thus only a Monte Carlo sampling of the measurand is possible [16]. If we define the probability distribution  $f_Y(y|\mathbf{a})$  that the measurand  $Y$  takes the value  $y$  given the set of conditions  $\mathbf{a}$  and a similar distribution  $f_Y(y|\mathbf{a}, y \geq 0)$  of a positive measurand, we can build the cumulative distribution function

$$F_Y(y|\mathbf{a}) = P(Y < y|\mathbf{a}) = \int_{-\infty}^y f_Y(\eta|\mathbf{a}) d\eta$$

and also

$$I_0 = \int_0^{\infty} f_Y(\eta|\mathbf{a}; y \geq 0) d\eta.$$

With these definitions, we can generalize the expressions for all the characteristic limits of the activity distribution given in section 1.1:

- the mean or expectation value  $\hat{y}$  is the best estimate for the measurand

$$\hat{y} = E(Y|\mathbf{a}, y \geq 0) = I_1/I_0; I_1 = \int_0^{\infty} y f_Y(y|\mathbf{a}) dy$$

- the standard uncertainty  $u(\hat{y})$  of the measurand associated with the best estimate  $\hat{y}$

$$u(\hat{y}) = \sqrt{E\left((Y - \hat{y})^2 | \mathbf{a}, y \geq 0\right)} = \sqrt{\frac{I_2}{I_0} - \hat{y}^2}$$

$$I_2 = \int_0^{\infty} y^2 f_Y(y|\mathbf{a}) dy$$

- the decision threshold  $y^*$  is the  $(1 - \alpha)$ -quantile of the  $f_Y(y|\tilde{\mathbf{a}}(\tilde{y} = 0))$ , i.e. of the distribution of an assumed true value  $\tilde{y} = 0$ . It is calculated by solving

$$1 - F_Y(y^*|\tilde{\mathbf{a}}(\tilde{y} = 0)) = \int_{y^*}^{\infty} f_Y(y|\tilde{\mathbf{a}}(\tilde{y} = 0)) dy = \alpha. \quad (\text{A.1})$$

This means that

$$P(y > y^*|\tilde{y} = 0) = \int_{y^*}^{\infty} f_Y(y|\tilde{\mathbf{a}}(\tilde{y} = 0)) dy = \alpha \quad (\text{A.2})$$

The decision threshold gives an indication whether the radioactivity is present. If the outcome of a measurement exceeds  $y^*$ , the measurand is potentially radioactive. If there is no real source, the error committed by assuming that it is radioactive is called error of the first kind or false positive error. The probability of committing such an error is exactly  $\alpha$  (that is commonly chosen to be 0.05). If the measured value  $y$  is below the decision threshold  $y^*$ , the result cannot be attributed to the physical effect, nevertheless it cannot be concluded that it is absent. If the physical effect is really absent, the probability of taking the wrong decision, that the effect is present, is equal to the specified probability,  $\alpha$  (probability of the wrong decision that it is not absent if it actually is)

- the detection limit  $y^\#$  is the assumed true value of the measurand if the decision threshold  $y^*$  is the  $\beta$ -quantile of  $f_Y(y|\tilde{\mathbf{a}}(\tilde{y} = y^\#))$ , i.e.

$$\begin{aligned} P(y < y^*|\tilde{y} = y^\#) &= F_Y(y^*|\tilde{\mathbf{a}}(\tilde{y} = y^\#)) \\ &= \int_{-\infty}^{y^*} f_Y(y|\tilde{\mathbf{a}}(\tilde{y} = y^\#)) dy = \beta. \end{aligned} \quad (\text{A.3})$$

The detection limit is the lowest activity that can be measured with a certain accuracy and with the applied measurement procedure. If the threshold is not exceeded, the error committed if a source is present is called error of the second kind or false negative error. The probability of such an error is  $\beta$  (that is commonly chosen to be 0.05). The detection limit,  $y^\#$ , is the smallest true value of the measurand, for which, the probability of the wrong decision, that the physical effect is absent if it is not, does not exceed the specified probability  $\beta$ . It is high enough compared to the decision threshold  $y^*$ , that the probability of a false negative decision does not exceed  $\beta$  and is obtained as the smallest solution of (A.3)

- the lower limit  $y^\triangleleft$  and upper limit  $y^\triangleright$  of the coverage interval are respectively the  $\gamma/2$ -quantile and the

$(1 - \gamma/2)$ -quantile of the density  $f_Y(y|\mathbf{a}, y \geq 0)$

$$\begin{aligned} F_Y(y^\triangleleft|\mathbf{a}, y \geq 0) &= \frac{\gamma}{2} = \frac{I_3}{I_0} \\ I_3 &= \int_0^{y^\triangleleft} f_Y(y|\mathbf{a}) dy = F_Y(y^\triangleleft|\mathbf{a}) - F_Y(0|\mathbf{a}) \end{aligned}$$

$$\begin{aligned} 1 - F_Y(y^\triangleright|\mathbf{a}, y \geq 0) &= \frac{\gamma}{2} = \frac{I_4}{I_0} \\ I_4 &= \int_{y^\triangleright}^0 f_Y(y|\mathbf{a}) dy = 1 - F_Y(y^\triangleright|\mathbf{a}). \end{aligned}$$

The coverage interval between the two limits defined above is such that it contains the true value of the measurand with the coverage probability  $1 - \gamma$  with  $\gamma$  commonly chosen to be 0.05. Using the Monte Carlo approach, the limits of the probabilistic symmetric coverage interval  $y^\triangleleft$  and  $y^\triangleright$  are the  $q_{\gamma/2}$  and the  $q_{1-\gamma/2}$  quantiles of the probability distribution  $f_Y(\tilde{y}|\mathbf{a})$  represented by the vector  $\mathbf{y}_M = \{y_1, \dots, y_{n_M}\}$  and taking into account that the measurand is non-negative. These quantiles can be conveniently calculated from the vector  $\mathbf{y}_M$  by searching the values  $y_{k_1} = y^\triangleleft$  and  $y_{k_2} = y^\triangleright$  with the conditions  $y_i \geq 0$ ,  $k_1/n_{M,1} = \gamma/2$  and  $k_2/n_{M,1} = 1 - \gamma/2$  where  $n_{M,1}$  is the number of elements in  $\mathbf{y}_M$  that are non-negative.